

Physical properties of $(\text{Mn}_{1-x}\text{Co}_x)\text{Si}$ at $x \simeq 0.06 - 0.1$: quantum criticality matter.

A. E. Petrova

*P. N. Lebedev Physical Institute, Leninsky pr., 53, 119991 Moscow, Russia and
Institute for High Pressure Physics of RAS, Troitsk, Russia*

S. Yu. Gavrilkin and G. V. Rybalchenko

P. N. Lebedev Physical Institute, Leninsky pr., 53, 119991 Moscow, Russia

Dirk Menzel

Institut für Physik der Kondensierten Materie, Technische Universität Braunschweig, D-38106 Braunschweig, Germany

I. P. Zibrov

Institute for High Pressure Physics of RAS, Troitsk, Russia

S. M. Stishov*

*P. N. Lebedev Physical Institute, Leninsky pr., 53, 119991 Moscow, Russia and
Institute for High Pressure Physics of RAS, Troitsk, Moscow, Russia*

We have grown and characterized three samples of Co doped MnSi and studied their physical properties (magnetization and magnetic susceptibility, heat capacity and electrical resistance). All three samples show non-Fermi liquid physical properties. From literature data and current results follow that impurities (Co and Fe) eliminate the first order phase transition peaks and spread the fluctuation maxima in such a way that its low temperature part effectively reaches the zero temperature, where the fluctuations inevitably become quantum. The behavior of low temperature branches of the heat capacity of the samples suggests that a gradual transition from classical to quantum fluctuations can be described by a simple power function of temperature with the exponent less than one. The $d\rho/dT$ data generally support this suggestion. The values of the heat capacity exponents immediately lead to the diverging ratio C_p/T and hence to the diverging effective electron mass. We found out that at large concentration of the dopant there are no distinct phase transition points. What we observe is a cloud of the helical fluctuations spreading over a significant range of concentrations and temperatures, which become quantum close to 0 K.

I. INTRODUCTION

Recent years the quantum critical phenomena in magnetic systems have attracted much attention. In a course of intensive studies, the helical magnet MnSi has played a special role as a material available in an almost perfect single crystal form, whose phase diagram and physical properties at high pressure were well known. As was shown in many studies the magnetic phase transition point in MnSi decreases with pressure and reaches almost zero at about 1.4 GPa¹⁻³. At the same time no evidence for quantum critical behavior were seen in MnSi at high pressure⁴⁻⁶. One of the reasons for this situation could be strong non hydrostatic stress developing at high compression⁵⁻⁷. To avoid this complication, it is reasonable to try using so called "chemical" pressure, which is replacing some atoms or ions of the material with chemically suitable atoms of smaller size. This procedure normally results in a volume decrease, which could imitate a high-pressure effect. Of course, it causes a certain disorder in materials that should be taken into account at the data interpretation. The described idea was used at studying the iron and cobalt doped of MnSi in Ref.⁸⁻¹⁰. As was shown in Ref.^{9,10} the iron doped sample of MnSi with a nominal composition $\text{Mn}_{0.85}\text{Fe}_{0.15}\text{Si}$ reveals features inherited to the proximity of quantum critical point. How-

ever, the results for Co doped samples, obtained in Ref.⁹, were not quite conclusive.

So, with all that in mind we decided to extend the study⁹ in relation of Co doped samples of MnSi.

II. EXPERIMENTAL

We prepared three samples with the nominal composition: $\text{Mn}_{0.94}\text{Co}_{0.06}\text{Si}$, $\text{Mn}_{0.92}\text{Co}_{0.08}\text{Si}$, $\text{Mn}_{0.9}\text{Co}_{0.1}\text{Si}$. Polycrystalline ingots containing Mn (Chempur; purity 99.99%), Co (Chempur; purity 99.95%), and Si ($\rho_n=300$ Ohm cm, $\rho_p=3000$ Ohm cm) were prepared by arc melting under argon atmosphere. Afterwards, single crystals have been grown using the triarc Czochralski technique.

The electron-probe microanalysis shows that real composition are: $\text{Mn}_{0.93}\text{Co}_{0.057}\text{Si}$, $\text{Mn}_{0.92}\text{Co}_{0.063}\text{Si}$, $\text{Mn}_{0.89}\text{Co}_{0.09}\text{Si}$, which indicates that two first samples have practically identical compositions despite the initial concentration of doping element (Table I).

We performed some magnetic, heat capacity and resistivity measurements to characterize the (Mn,Co)Si samples. All measurements were made making use the Quantum Design PPMS system with the heat capacity and vibrating magnetometer moduli and the He-3 Refrigerator. The resistivity data were obtained with the standard

TABLE I: Chemical compositions and lattice parameters of (Mn,Co)Si, (Mn,Fe)Si and MnSi samples. a -lattice parameter, V -unit cell volume.

| Nominal composition | Electron-probe Composition | a Å | V Å ³ |
|--|--|----------|-----------------------|
| Mn _{0.94} Co _{0.06} | Mn _{0.93} Co _{0.057} Si ^a | 4.5522 | 94.333 |
| Mn _{0.92} Co _{0.08} Si | Mn _{0.92} Co _{0.063} Si ^a | 4.5519 | 94.313 |
| Mn _{0.9} Co _{0.1} Si | Mn _{0.89} Co _{0.09} Si ^a | 4.5499 | 94.189 |
| Mn _{0.85} Fe _{0.15} Si | Mn _{0.83} Fe _{0.17} Si ^b | 4.5462 | 93.961 |
| MnSi | MnSi ^c | 4.5598 | 94.8063 |

^aCurrent paper.

^bRef.¹⁰, (Chemical composition data in the table obtained in new facilities are slightly different from Ref.¹⁰)

^cRef.¹¹.

four terminals scheme using the spark welded Pt wires as electrical contacts.

The experimental data are shown in Fig. 1–8.

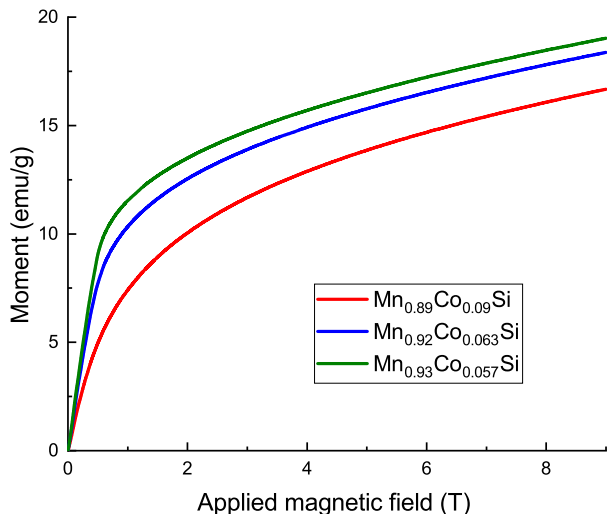


FIG. 1: (Color online) Magnetizations of samples (Mn,Co)Si at 2 K.

Fig. 1 illustrates magnetization of the samples in the fields to 9 T. As is seen there are no indications for spontaneous magnetic moments in these materials.

The magnetic susceptibility of (Mn,Co)Si samples is demonstrated in Fig. 2. in the limited range of temperature for a better viewing of the specific features of these cobra-like curves. At the first sight these cobra-like features are nothing else than strongly deformed maximum of $\chi(T)$ observed in the pure MnSi at the phase transition point. Similar maxima in $\chi(T)$ were seen in⁹ at lower Co concentrations. If these maxima indeed correspond to the "phase transition" points it worth comparing the data with the results of Ref.⁹ that will be done lately in this paper.

The results of heat capacity measurements are displayed in Fig. 3. As is seen in Fig. 4 the lines of $C_p(T)$

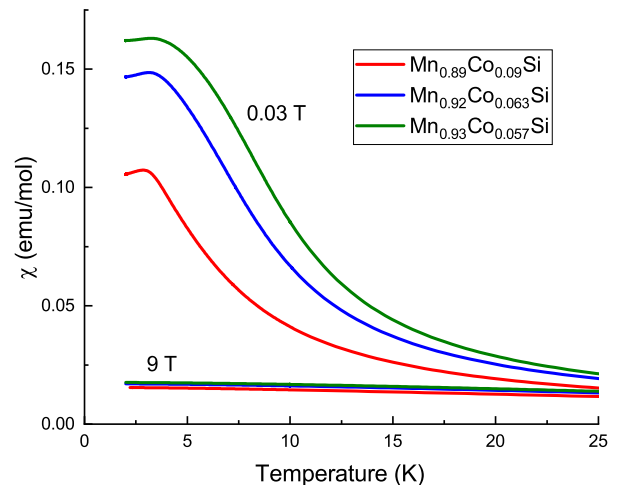


FIG. 2: (Color online) Magnetic susceptibility of (Mn,Co)Si as a function of temperature at 0.03 and 9 T.

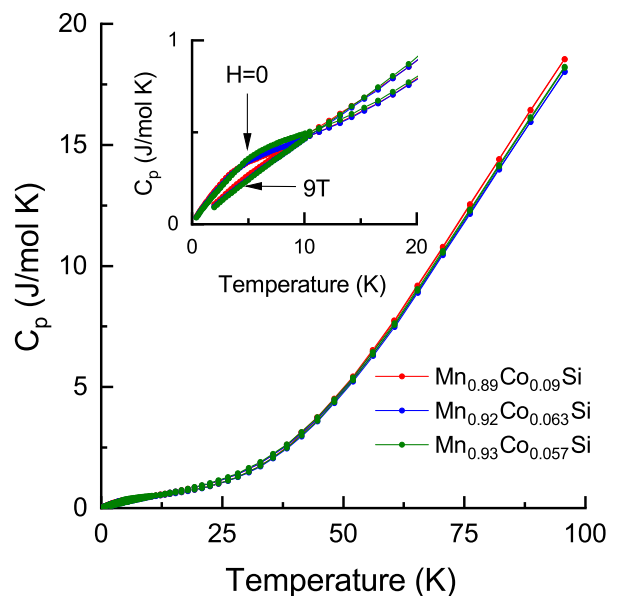


FIG. 3: (Color online) Heat capacity of (Mn,Co)Si at zero and 9 T as a function of temperature in the range 0.4–100 K. Enlarge part of the plot is in the inset.

changes their slope rather sharply at temperatures in the vicinity of 4–5 K. Actually, these features can be attributed to the strongly smeared out the fluctuation induced heat capacity maximum associated with the magnetic phase transition in pure MnSi.

The mentioned slope change, which becomes more evident after a subtraction from the heat capacity curve at zero magnetic field the corresponding curve at 9 T, occurs at ~ 5 K (Mn_{0.93}Co_{0.057}Si), ~ 4.7 K (Mn_{0.92}Co_{0.063}Si) and ~ 3.4 K (Mn_{0.89}Co_{0.09}Si) (Fig. 5). Actually, this manipulation implies a subtraction of some of background contributions, including phonon one to the heat capacity leaving its fluctuation part intact. At the same time as

seen in Fig. 5 this procedure reduces the low temperature branch of the C_p to the puzzling universal line even including data on MnFeSi^{10} . On the other hand, the high temperature branches of the differential C_p curves became negative at some temperatures therefore supporting our old conclusion that strong fluctuations give negative contributions to the heat capacity of paramagnetic phase of MnSi^{11} .

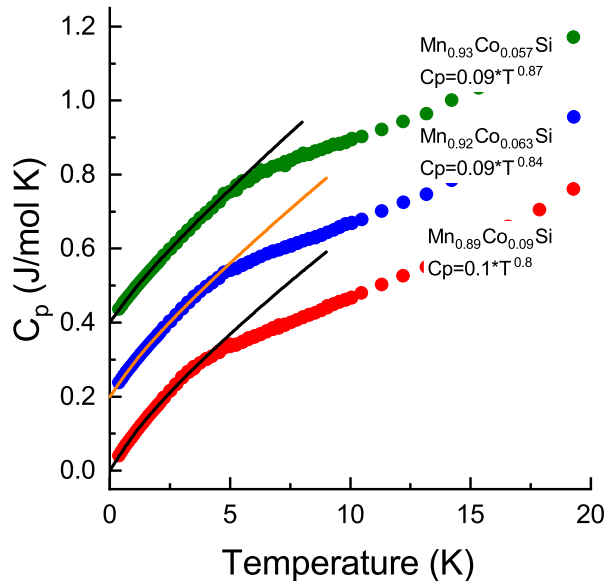


FIG. 4: (Color online) Illustration to the fitting of the low temperature part of heat capacity to the power function. The values of the power exponents shown in the plot. The data are shown with offsets for better viewing.

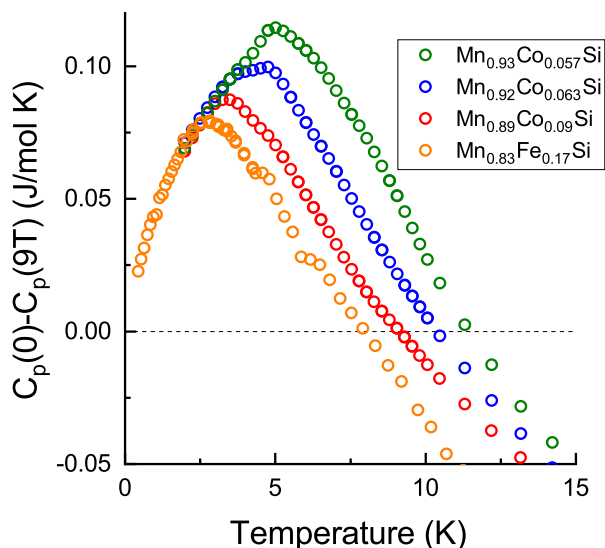


FIG. 5: (Color online) The difference between heat capacity at zero magnetic field $C_p(0)$ and heat capacity at 9 T ($C_p(9T)$) for (Mn,Co)Si samples (current work) and one sample of (Mn,Fe)Si¹⁰.

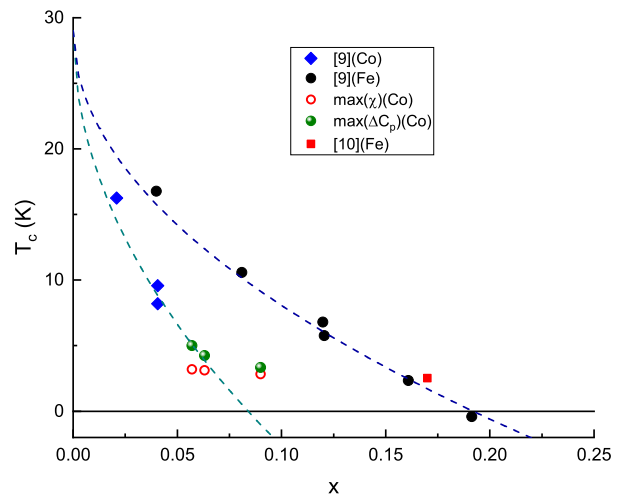


FIG. 6: (Color online) "Phase transition" temperature as a function of concentrations for $\text{Mn}_{1-x}\text{Fe}_x\text{Si}^{9,10}$ and $\text{Mn}_{1-x}\text{Co}_x\text{Si}^9$ and current data. Indications of chemical elements in legend show nature of dopants. In Ref.⁹ "phase transition" temperatures were determined from the temperature dependence of magnetic moments. Current data were taken as the χ maxima (Fig. 2) and maxima of $\Delta C_p(0 - 9T)$ (Fig. 5). Note that the square datapoint on the "iron" curve corresponds to the sample studied in¹⁰ (Corrected composition was used. Transition temperature was taken as a maximum of $\Delta C_p(0 - 9T)$ (Fig. 5)).

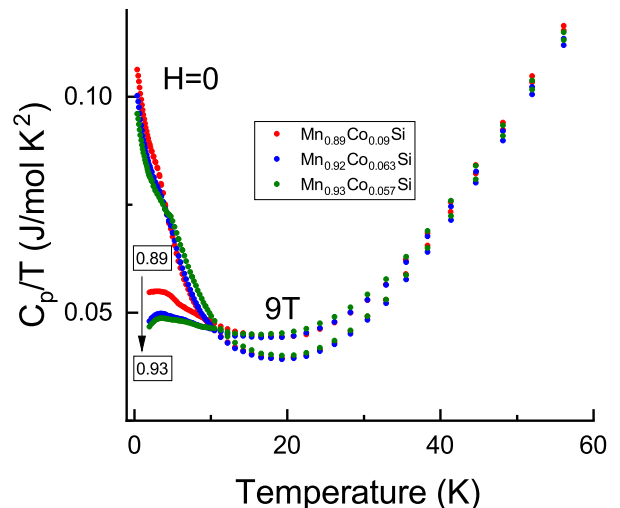


FIG. 7: (Color online) The ratio C_p/T for (Mn,Co) samples as a function of temperature at zero and 9 T magnetic fields. It is seen that diverging of C_p/T is suppressed by strong magnetic field.

The maximum temperatures of the curves in Fig. 5 generally correlate with the local maxima of $\chi(T)$ taken as the "phase transition" temperatures (see Fig. 2). In Fig. 6 is seen that data points with concentration $x \approx 0.06$ fit well with data of Ref.⁹, whereas the ones with $x = 0.09$ sharply deviates from the suggested curve. Moreover, an impression arises that the "phase transi-

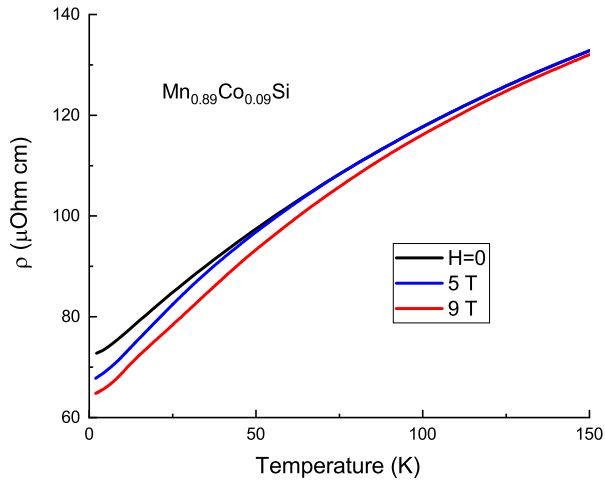


FIG. 8: (Color online) The dependence of resistivity of $\text{Mn}_{0.89}\text{Co}_{0.09}\text{Si}$ on temperature at various magnetic fields.

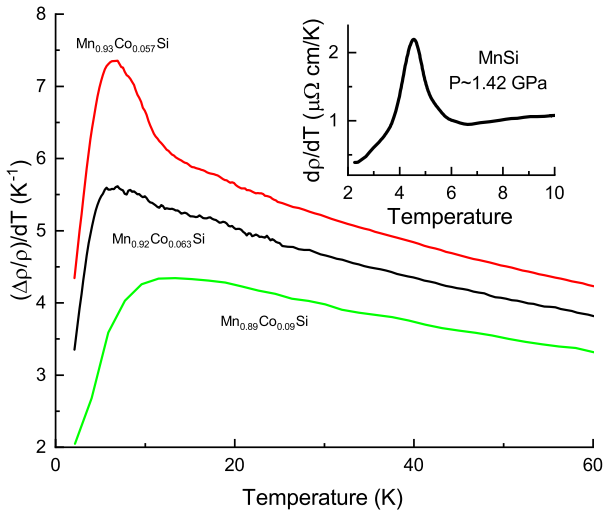


FIG. 9: (Color online) Temperature derivatives of resistivity of the samples $\text{Mn}_{1-x}\text{Co}_x\text{Si}$. In the inset $d\rho/dT$ data for pure MnSi at the phase transition occurring at high pressure are shown (after Ref.¹⁵).

tion” temperature somehow avoids declining at further increasing of Co concentration.

Anyway, the low temperature branches of the heat capacity curves reflect a gradual transition from classical to quantum fluctuations, which can be described by a simple power function of temperature with the exponent less than one. The latter immediately leads to the diverging ratio C_p/T (see Fig. 7) and hence to the diverging effective electron mass, which is a signature of the quantum critical behavior.

The resistivity of the samples as a function of temperature exhibits an evolution from low temperature region of not quite clear underlying physics to the ”saturation” regime typical of the strongly disordered metals¹² (Fig. 8 (see also Ref.¹⁰)).

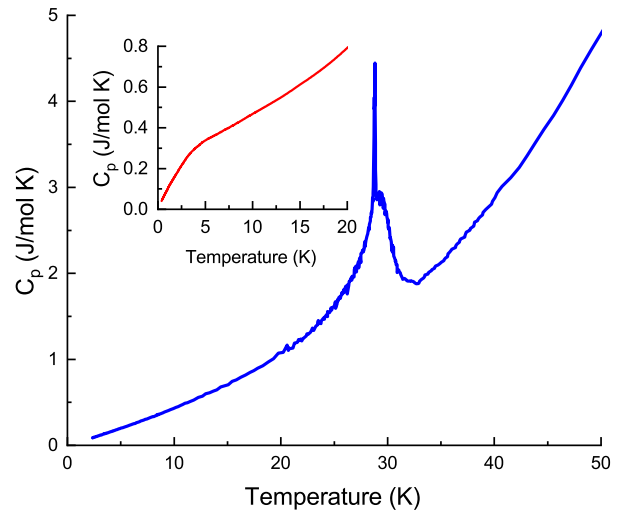


FIG. 10: (Color online) Temperature dependence of heat capacity near the magnetic phase transition in MnSi (after Ref.¹⁵). In the inset heat capacity anomaly in $\text{Mn}_{0.89}\text{Co}_{0.09}\text{Si}$ is shown.

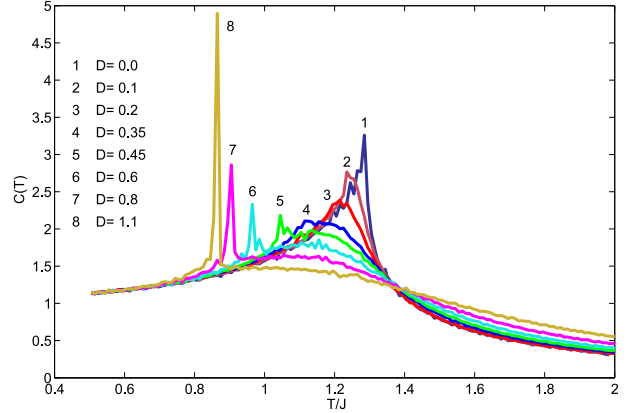


FIG. 11: (Color online) Temperature dependence of the specific heat $C(T)$ for the Hamiltonian $H = H_J + H_D$ for different values of the DM (D)interaction (after Ref.¹⁶).

Fig. 8 illustrates this kind of the resistivity behavior in magnetic field to 9 T using the sample $\text{Mn}_{0.89}\text{Co}_{0.09}\text{Si}$ as a typical example. In attempt to understand the low temperature conduct of the resistivity we performed a fitting of the corresponding data with the expression $\rho = A + BT^n$ in the range 2-8 K. The following values of exponents n were obtained: $n = 1.7$ ($H = 0$), $n = 1.4$ (5 T), $n = 1.6$ (9 T), which uncovers non-Fermi-liquid behavior. This finding adds one more puzzle to the problem of non-Fermi-liquid exponent^{12,13}.

Temperature derivatives of resistivity of the samples $\text{Mn}_{1-x}\text{Co}_x\text{Si}$. Are displayed in Fig. 9. These data correlate in certain aspects with those shown in Fig. 4, 5 identifying the low temperature parts of the corresponding curves with the smeared out low temperature sides of the fluctuation maxima (see the inset where $d\rho/dT$ data for the high pressure phase transition in pure MnSi are

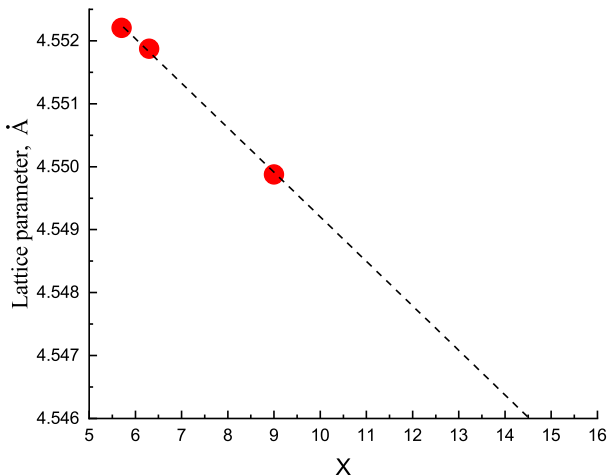


FIG. 12: (Color online) Lattice parameter of $\text{Mn}_{1-x}\text{Co}_x\text{Si}$ as a function of Co concentration (X) (Table I).

demonstrated).

III. DISCUSSION

First, let us to turn attention to Fig. 10, demonstrating a behavior of heat capacity in pure MnSi at the magnetic phase transition¹⁵. As can be seen in Fig. 10 the phase transition in MnSi is characterized by a sharp peak on top of a rounded maximum forming a shoulder in the high temperature side of the peak. According to the Monte Carlo calculations¹⁶ such structure of the heat capacity results from the perturbation of a virtual second order ferromagnetic phase transition by the helical fluctuations, which smeared out the transition and eventually condense into the helically ordered phase (see Fig. 11).

From the data⁹ and the current results follow that impurities (Co and Fe) extinguish the first order peaks and spread the fluctuation maxima in such a way that its low temperature part effectively reaches the zero temperature, where the fluctuations inevitably become quantum (see Fig. 5). Moreover, a doping action of Co, obviously saturates at some concentrations, so the χ and $C_p(0) - C_p(9T)$ maxima do not move significantly with concentration increasing (Fig. 2, 5). Note that in Ref.¹⁰ the quantum critical trajectory was identified for the sample $\text{Mn}_{0.83}\text{Fe}_{0.17}\text{Si}$ with a lattice parameter 4.5462 Å, the value, which coincides with the lattice parameter of pure MnSi at the phase transition point at $T \sim 0$ K and $P \sim 14.5$ kbar. Follow this reason, we plot available lattice parameter data of (Mn,Co)Si as a function of Co concentration (Fig. 12). The extrapolation by the Vegard's rule shows that the value of lattice parameter equal to

4.5462 Å for (Mn,Co)Si can be attained at 14-15 % concentration of Co i.e. at composition $\text{Mn}_{0.85}\text{Co}_{0.14-0.15}\text{Si}$. However, it is not clear whether this concentration is reachable. Moreover, in the light of the current study one hardly can find a unique single critical trajectory. Probably the same should be applicable to the $\text{Mn}_{1-x}\text{Fe}_x\text{Si}$ case. So, the conclusion of Ref.¹⁰ may be need a modification.

Thus, at large concentrations of the dopant there is no a definite phase transition point, instead one has a cloud of the helical fluctuations, which spread over a significant range of concentrations and temperatures and become quantum close to 0 K. Diverging the ratio C_p/T justifies this fact and leads to infinite electronic effective mass as a signature of quantum criticality (Fig. 7).

IV. CONCLUSION

We have grown and characterized three samples of Co doped MnSi and studied their physical properties (magnetization and magnetic susceptibility, heat capacity and electrical resistance). All three samples show non-Fermi liquid physical properties. From the data⁹ and current results follow that impurities (Co and Fe) eliminate the first order phase transition peaks and spread the fluctuation maxima in such a way that its low temperature part effectively reaches the zero temperature, where the fluctuations inevitably become quantum (see Fig. 4,5). The behavior of low temperature branches of the heat capacity of the samples (Fig. 4,5) suggests that a gradual transition from classical to quantum fluctuations can be described by a simple power function of temperature with the exponent less than one. The $d\rho/dT$ data generally support this suggestion (Fig. 12). The value of the heat capacity exponents immediately leads to the diverging ratio C_p/T (see Fig. 7) and hence to the diverging effective electron mass. We found out that at large concentration of the dopant there are no distinct phase transition points (Fig. 2,5). What we observe is a cloud of the helical fluctuations spreading over a significant range of concentrations and temperatures, which become quantum close to 0 K (Fig. 6).

V. ACKNOWLEDGEMENTS

The authors gratefully acknowledge the technical support of Dr. V.A. Sidorov. AEP and SMS greatly appreciate financial support of the Russian Foundation for Basic Research (grant No. 18-02-00183) and the Russian Science Foundation (grant 17-12-01050).

* Electronic address: stishovsm@lebedev.ru

¹ J. D. Thompson, Z. Fisk, and G. G. Lonzarich, Physica B

- 161**, 317 (1989).
- ² C. Pfleiderer, G. J. McMullan, and G. G. Lonzarich, *Physica B* **206-207**, 847 (1995).
 - ³ C. Thessieu, J. Flouquet, G. Lapertot, A. N. Stepanov, D. Jaccard, *Solid State Commun.* **95**, 707 (1995).
 - ⁴ C. Pfleiderer, P. Böni, T. Keller, U.K. Rössler, A. Rosch. *Science*, **136**, 1831 (2007).
 - ⁵ S.M. Stishov, A.E. Petrova, *Physics–Uspekhi* **54**, 1117 (2011).
 - ⁶ A.E. Petrova, S.M. Stishov, *Phys.Rev. B* **86**, 174407 (2012).
 - ⁷ A.M. Belemuk, S.M. Stishov, *J.Phys.: Condens. Matter* **31**, 135801 (2019).
 - ⁸ C. Meingast, Q. Zhang, T. Wolf, F. Hardy, K. Grube, W. Knafo, P. Adelman, P. Schweiss, H. v. Löhneysen; V. Zlatić, A. C. Hewson (eds.), *Properties and Applications of Thermoelectric Materials*, 261 NATO Science for Peace and Security Series B: Physics and Biophysics, Springer Science-Business Media B.V. (2009).
 - ⁹ A. Bauer, A. Neubauer, C. Franz, W. Münzer, M. Garst, C. Pfleiderer, *Phys.Rev. B* **82**, 064404 (2010)
 - ¹⁰ A. E. Petrova, S. Yu. Gavrilkin, Dirk Menzel, S. M. Stishov, *Phys.Rev. B* **100**, 094403 (2019)
 - ¹¹ S. M. Stishov, A. E. Petrova, A. A. Shikov, Th. A. Lograsso, E. I. Isaev, B. Johansson, and L. L. Daemen, *PRL* **105**, 236403 (2010)
 - ¹² H. Wiesmann, M. Gurvitch, H. Lutz, A. Ghosh, B. Schwarz, M. Strongin, P. B. Allen, and J. W. Halley, *Phys. Rev. Lett.* **38**, 782 (1977).
 - ¹³ G.R. Stewart, *Rev. Mod. Phys.* **73**,797 (2001)
 - ¹⁴ M. Brando, D. Belitz, F.M. Grosche, T.R. Kirkpatrick, *Rev.Mod.Phys.* **88**, 025006 (2016)
 - ¹⁵ S. M. Stishov, A. E. Petrova, S. Khasanov, G. Kh. Panova, A. A. Shikov, J. C. Lashley, D. Wu and T. A. Lograsso, *J. Phys.: Condens. Matter* **20**, 235222 (2008)
 - ¹⁶ A. M. Belemuk and S. M. Stishov, *Phys. Rev. B* **95**, 224433 (2017)